BIOMECHANICAL MODEL OF PREGNANT FEMALE FOR IMPACT PURPOSES

Magdalena Jansová*, Luděk Hynčík**

Biomechanics has widely expanded in the last decades. The fast development of computers provides new possibilities in this field. Problems can be solved faster and can be more extensive. One of these problems is the biomechanical model of human body. Its realisation is practically impossible without using computers, because it is necessary to solve systems of thousands of equations.

There are several software packages that enable human body modeling. One of them is the PAM environment [15] developed by the ESI Group International. This computational system is based on the Finite Element Method and is one of the mostly used systems for crash test simulations.

Various human body models for various purposes are developed. Pregnant female model serve to optimize safety systems in cars to be more friendly to pregnant abdomen.

Key words : *human model, pregnant female, validation, impact*

1. Introduction

The aim of this study is the creation of deformable finite element biomechanical pregnant female model within the PAM environment. This model upgrades the *ROBINA* female human articulated body model developed in [10]. Since the main focus is the pregnant abdomen model, the abdomen and the upper part of the legs close to the abdomen are deformable. The head, extremities and thoracic bones are rigid. The abdominal model has been created with respect to the CT data of pregnant female [22]. Other source of data was the Visible Human Project [23]. The model was completed by the choice of the material models, specification of the material properties and definition of contacts between particular organs. The pregnant female abdomen model is validated on Cavanaugh frontal test and INRETS experimental tests. The practical application of the pregnant female model is demonstrated on several types of sled tests focused on optimization of the safety systems.

2. Used methodology

2.1. Finite elements

The tissues modeled in pregnant female model, and generally in human model by [9], can be divided into two groups – thin and thick. Thin tissues are modeled by two-dimensional membrane or shell elements, thick tissues are modeled by three-dimensional solid elements.

* Ing. Magdalena Jansová, Ph.D., Department of Mechanics, Faculty of Applied Sciences, University of West Bohemia, Univerzitní 22, 306 14 Plzeň, Czech Republic

** Ing. L. Hynčík, Ph.D., New Technologies – Research Centre in the Westbohemian Region, University of West Bohemia, Univerzitní 22, 306 14 Plzeň, Czech Republic

The organs can be divided into solid and hollow organs. Solid organs are modeled by three-dimensional solid elements. These elements take the form of tetrahedrons, pyramids, pentahedrons and hexahedrons. The hollow organs are filled by a fluid, which can be modeled by three-dimensional solid elements or by biobags [9].

In biological reality some organs are covered by thin membranes. They usually do not have considerable mechanical properties, but can be used as contact surfaces in definitions of contact interfaces. Shell and membrane elements are triangular and quadrilateral. The shell elements have bending and transverse shear effects but they can be degenerated to membrane elements without these effects. The shell elements can be compared to a thin plate, the membrane elements behave like fabric.

When creating the model, it is important to distinguish the minimal size of any tissue according to [12, 15]. All element sizes should not decrease under the given size since the reasonable time step. The consequence is that the real shapes of tissue have to be simplified. The time step should be compatible for further simulation of the human model with surrounding structure for the explicit solver [9, 15]. The advantage of hexahedral elements is a significantly higher time step in comparison to that of tetrahedral element with the same edge size.

2.2. Biobags

Biobag models are derived from airbag model, that is provided by the solver [9, 15]. The advantage of using biobag model is that the fluid has only its state characteristics which are constant over its volume which is surrounded by the biobag surface and there are no finite elements for the fluid inside. It results in faster computation.

2.3. Rigid bodies

The abdomen and the upper part of the legs close to the abdomen are deformable. The head and extremities are rigid, because they have no significant influence on the abdomen and this simplification saves computational time. The ribs and sternum form next rigid body. The bones of shoulder (clavicula and scapula) are rigid as well. The rigid body is defined by its geometry (parts, elements and nodes), the centers of gravity and the moments of inertia. They were computed for each rigid body by a simple program in *MATLAB* as introduced in [9]. The motion of the rigid body is determined by the motion of its center of gravity. It consists of translations and rotations. The boudary conditions that we want to apply to the rigid body must be applied to its center of gravity only.

2.4. Kinematic joints

The joints between the particular rigid bodies are represented by kinematic joints corresponding to a nonlinear spring and dashpot element connecting two nodes [15]. In pregnant female model, there is mainly used spherical type with nodes equal to each other.

2.5. Mutual contacts

The organs may move under the influence of force activity which could result in the penetration of particular organs. To avoid this, it is necessary to define mutual contacts among the individual parts of the model. The contacts modeled inside the human body can be divided into connections that supply the ligaments and sliding contacts that are present in biological reality.

The sliding contact is defined by definition of master and slave surfaces and the contact thickness at which the contact is initiated [15]. The ligaments and tied connections are simulated by tied interface. For this interface, the slave nodes can be tied at a certain distance from the master surface [15].

3. Creation of pregnant female model

The whole pregnant female model is based on Finite Element Method. It is generated according to real anatomical data by virtue of *Amira* software from Mercury Computer Systems, Inc. [20] and *HyperMesh*® software from Altair Engineering, Inc. [19]. It is created for further use in the PAM environment [15].

3.1. Abdomen

The model of inner abdominal organs is based on the only available CT data of a pregnant woman obtained from [22]. The woman was 30 weeks pregnant and the CT scan covered the portion of the body between the lower breast and the hip in 70 slices, each 7 mm thick.

The CT data were loaded into software *Amira* and the boundaries of particular organs were manually drawn on each picture. These boundaries were used for generation of triangular surface mesh covering each organ.

Created meshes and the *ROBINA* model [1, 10] were loaded into *HyperMesh*® software. Tetrahedral grids of abdominal organs were translated, rotated and scaled to fit to the bones of the *ROBINA* model. For the proper placing of organs, it was used the fitting of created mesh of pelvis into already existing *ROBINA* pelvis. The shape and proportions of the organs have been confronted with the anatomical books [4, 18]. The skin of the *ROBINA* model was modified according to the discussion with physician to agree with the look of pregnant female.

The hexahedral mesh of each organ (Fig. 1), based on the tetrahedral model resulting from *Amira* and consulted with [4, 18], was created manually in *HyperMesh*® software. Pentahedrons, pyramids and tetrahedrons were used only where it was really necessary. The organs were covered by diaphragm and peritonemum according to [18].

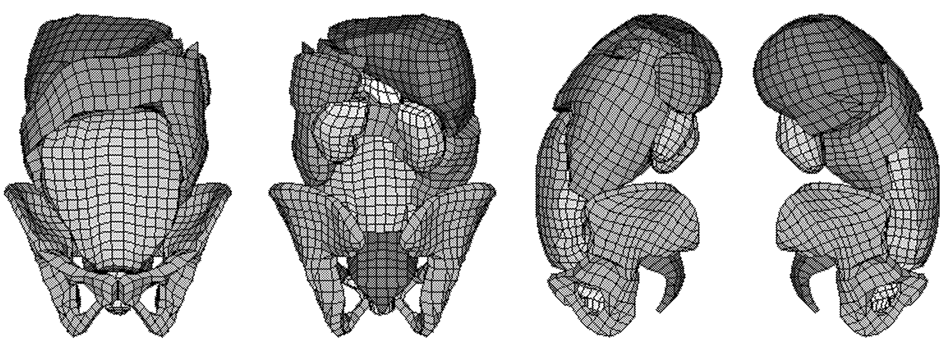

Fig.1: Hexahedral model of pregnant female abdomen and pelvis – frontal, rear, left and right aspect

The model of the liver had to be modified slightly on the lateral side, because the liver tissue should not be lower than the ribs (according to the discussion with physicians). The mesh of adrenal glands did not correspond to the physiological state and therefore it was situated on the top of each kidney that should correspond to the physiological state. The ovaries were not used in the abdominal model further since their size is small. The intestines are formed by a long tube but this structure was not preserved in the pregnant female model and the intestines were modeled as one solid organ (see Fig. 1) [9].

Because the pelvis historically used in the *ROBINA* model was not a typical female pelvis, a new model of pelvis was reconstructed in *Amira* from the CT data of a female obtained from Visible Human Project® [23]. The pelvis model was scaled to fit into *ROBINA* model and the os sacrum was remeshed into hexahedrons according to the os sacrum in *ROBINA* model (see Fig. 1). Hexahedral model of spine was created according to [18]. The vertebrae were connected with each other by intervertebral discs (see Fig. 4).

The pregnant female model was seated into the seat used for sled tests with the *ROBBY2* model [9]. Each tissue was renamed and renumbered according to the names and numbers used in the *ROBBY2* model [1, 9]. The nodes and elements were renumbered according to the system used in [9]. The materials and material parameters of particular tissues, except of the uterus, were obtained via common collaboration with ESI Group.

3.1.1. Uterus

The uterine model is 20 cm long, 18 cm wide and 9 cm deep. The cervix is about 1.5 cm long. The weight of the uterine wall tissue is 0.76 kg and the content weights 1.3 kg. The muscular layer of the uterine wall is modeled by one layer of solid elements (see Fig. 2). The uterine wall thickness during pregnancy was measured by Degani et al. [5] in various segments. The uterus model is simplified and has the same thickness for all segments. The dependencies of uterine wall thickness on the week of pregnancy were displayed for each segment. The uterine wall thicknesses at 30 weeks of pregnancy were obtained from these dependencies and their mean value, 8.87 mm, was used in the uterus model. The serosal layer and the mucosal layer are not modeled because it is supposed that they have no significant influence on the mechanical response of the uterine wall tissue.

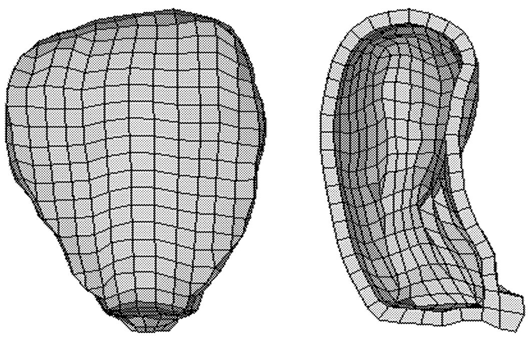

Fig.2: Hexahedral uterine model – frontal aspect and medial cross-section

Two different material models are used for modeling the uterine wall tissue. The first material model used is elastic-plastic material for solid elements (material type 1) provided by the solver [15]. The elastic behaviour of this material is defined by the shear modulus

$$G = \frac{E}{2\,(1+\nu)} \tag{1}$$

and the bulk modulus

$$K = \frac{E}{3\,(1-2\,\nu)}\ , \tag{2}$$

where E denotes Young's modulus and ν Poisson's ratio. The mass density, Young's modulus and Poisson's ratio are found in [14] (Table 1). The values of the shear modulus and the bulk modulus calculated from equations (1) and (2) are in Table 2. The plastic behaviour is defined in the way that the material corresponds to the linear elastic.

Structure	**Material model**	ρ [kg/m^3]	E [kPa]	ν
Uterus	Linear Elastic	1052	566	0.40

Tab.1: Material properties used for the pregnant uterus model (taken from [14])

Parameter	**Size** [GPa]
Shear modulus	2.02×10^{-4}
Bulk modulus	9.43×10^{-4}

Tab.2: Material parameters of elastic-plastic material

The second material model used is the visco-elastic material (material type 22) for solid elements [15]. The material properties of this material are identified using data available from the experiment [13].

The linear elastic modulus of the viscous part is set to very high value ($E\times10^5$) so that the whole Zener model behaves as Kelvin model. The mass density has the same value as for elastic-plastic material. The Poisson's ratio is set to 0.49, because the uterine tissue is supposed to be almost incompressible.

Parameter	**Mean value**	**Deviaton**
E [10^4 N/m^2]	2.6674	0.3346
η [10^4 Pa.s]	6.4428	0.7928

Tab.3: Material parameters for visco-elastic material

The uterine surface is covered by a layer of shell elements of material without any mechanical serving as contact surface, so called null material [15].

As mentioned in [6, 14], the uterus can be modeled without the fetus inside that can be substituted by the amniotic fluid. That lead to the idea of replacing the contents of the uterus by a biobag [9]. The interior of the uterine wall is covered by a layer of membrane elements serving as the envelope of a biobag. The mass of the biobag is set so that the density of the fluid inside corresponds to the density of the amniotic fluid which is equal to 993 kg/m^3 as found in [14].

The cervix should be modeled as hollow. However the use of biobag does not allow it because in that case the cervix is inflated by the biobag content due to the initial pressure. Therefore the solids forming the cervix are firmly connected to each other.

Other external or internal female reproductive organs are substituted by the flesh (see section 3.3).

3.2. Thorax

The model of thorax consists of several parts. The thoracic flesh is modeled as described in the section 3.3. The rib cage consisting of the ribs and sternum is modeled as rigid. The thoracic organs are substituted by a biobag. The mass of the biobag is set as the total mass of the heart (250 g), the left lung (565 g) and the right lung (625 g), which is equal to 1.440 g. The masses of particular organs were found in [18].

3.3. Flesh and skin

In biological reality there are three layers between organs ant the body surface – fat layer, muscular layer and skin layer. For pregnant female model are all three layers considered homogeneous and modeled by one type of material [9].

The solid elements fill in the space between the organs and bones and the body surface. The pregnant female model is oriented mainly at the proper model of the pregnant abdomen. Therefore the abdominal flesh is created predominantly in hexahedrons. The thoracic flesh and the flesh of the neck are formed by tetrahedrons beacuse they can be created automatically in *HyperMesh*® software.

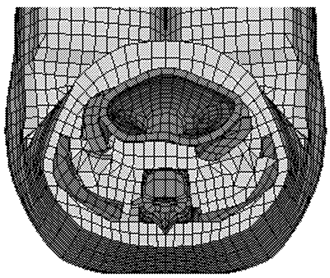

Fig.3: Flesh (light) and other tissues (dark) – abdominal cross-section

The abdominal and thoracic flesh is modeled using the hyperelastic Hart-Smith material for solid elements [15]. The flesh of the neck is modeled using the linear visco-elastic material for solid elements [15]. The outer surface of the flesh is covered by a fabric membrane elements with nonlinear fibers [15] replacing the skin. The inner surface of the flesh is covered by a layer of shell elements of the null material. The material parameters were obtained via common collaboration with ESI Group.

3.4. Head and extremities

Since the original *ROBINA* bones of lower limbs were slightly unproportional, new bones were reconstructed in *Amira* from the CT data of a female obtained from Visible Human Project® [23].

The bones of foot and low leg, patella and lower part of femur are left as the shell triangular elements resulting from *Amira*, because they are defined as parts of rigid bodies (see Fig. 4 left). The upper part of femur femur was created in two variants. In the first one the femur is formed by the shell triangular elements for use as rigid model of femur. The second variant is manually remeshed deformable solid model of femur with shell elements on the surface (see Fig. 4 right). The resulting models are mirrored to obtain the models of the other leg.

Fig.4: Meshed model of the spine (left), bones of the left leg (middle) and detail of femur (right) with deformable upper part and rigid lower part

The model of head and upper extremities and the skin of lower extremities is taken from the *ROBINA* model. The model of the head is formed by one rigid body. It is composed of eleven parts including the head surface and the bones. The model of each upper and lower extremity is formed by three rigid bodies – the upper part, the lower part and the hand/foot. Each is composed of the skin and particular bones. Between each rigid body is the connection that is not rigid and allows the skin modification while movement of the joints. The part of the lower extremity close to the abdomen is deformable and is not involved in the upper part rigid body [9]. The material parameters were obtained via common collaboration with ESI Group.

4. Model validation

According to quasi-static testing of pregnant and non-pregnant abdomens performed in [16], the quasi-static stiffness of the pregnant abdomen is not significantly different from the non-pregnant female abdomen and the male abdomen.

4.1. Data filtering and normalization

The curves are filtered in *HyperView*® environment by batch filter. It uses a Fast Fourier Transform to trasform the data into the frequency domain. The data are then filtered through an ideal filter with low and high cutoff frequencies, and transformed back into the time domain by inverse Fast Fourier Transform.

In order to normalize the data is used an equal stress – equal velocity scaling method described in [7, 8]. The scaling factor λ results from the following equation:

$$\lambda = \left(\frac{76\,\mathrm{kg}}{\text{body mass of tested subject}} \right)^{\frac{1}{3}} . \tag{3}$$

The force and deflection is scaled as

$$F = \lambda^2 \, F_\mathrm{m} \ , \qquad D = \lambda \, D_\mathrm{m} \ , \tag{4}$$

where F_m and D_m are force and deflection resulting from computation and F and D are normalized values. The body mass of pregnant female model is equal to 60.5 kg that results in λ equal to 1.0788.

4.2. Cavanaugh frontal test

The pregnant female abdominal model is validated on Cavanaugh frontal test based on an experiment described in [3]. The abdomen is impacted in a frontal direction at the level of the L3 vertebra by a rigid bar with diameter 25 mm (length equal to 381 mm) and mass equal to 32 kg and 64 kg respectively.

The test is performed for rigid bar initial speed equal to 6.1 m/s and 10.4 m/s. Since there is not clear which rigid bar mass was used for particular speed, the test is performed for all combinations. The deformable variant of femur is used. Fig. 5 shows the test setup.

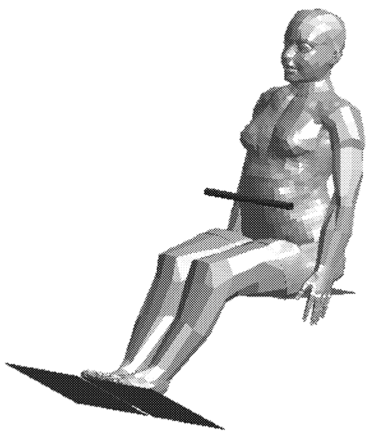

Fig.5: The Cavanaugh frontal test setup

The resulting deflection-force dependencies are not filtered, because the initial force peak caused that the beginning of the curves after filtration does not correspond to the original curve. The peak is caused probably by the numerical initial instability of the model.

The deflection-force dependence for the frontal test with speed equal to 6.1 m/s and uterus modeled using material type 1 shows linear dependence between the rigid bar penetration and abdominal force response for both masses of the rigid bar (see Fig. 6 left). Both dependencies are almost the same, the higher rigid bar mass affects the longer evolution of the dependence leading to the hiher values of the force. The plateau corresponding to the Cavanaugh corridor is visible.

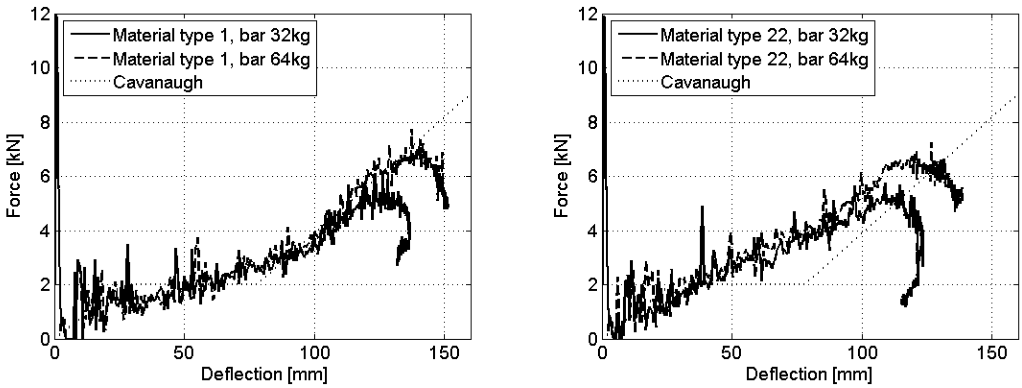

Fig.6: Results of the Cavanaugh frontal test, speed equal to 6.1 m/s, uterus modeled using material type 1 (left) and material type 22 (right)

The deflection-force dependence for the frontal test with speed equal to 6.1 m/s and uterus modeled using material type 22 shows linear dependence between the rigid bar penetration and abdominal force response for both masses of the rigid bar (see Fig. 6 right). Both dependencies are almost the same until the deflection reaches approximately 90 mm, when the higher rigid bar mass causes the slight increase of the force and the longer evolution of the dependence.

The force during the frontal test performed with speed equal to 6.1 m/s has bigger value for uterus modeled using material type 22 compared to the one for uterus modeled using material type 1. On the other hand the usage of material type 1 leads to the curve with more significant plateau corresponding to the Cavanaugh corridor.

The deflection-force dependence for the frontal test with speed equal to 10.4 m/s and uterus modeled using material type 1 shows linear dependence between the rigid bar penetration and abdominal force response for both masses of the rigid bar (see Fig. 8 left). Both dependencies are almost the same until the deflection reaches approximately 120 mm, when the higher rigid bar mass causes the slight increase of the force and the longer evolution of the dependence. The plateau corresponding to the Cavanaugh corridor is visible.

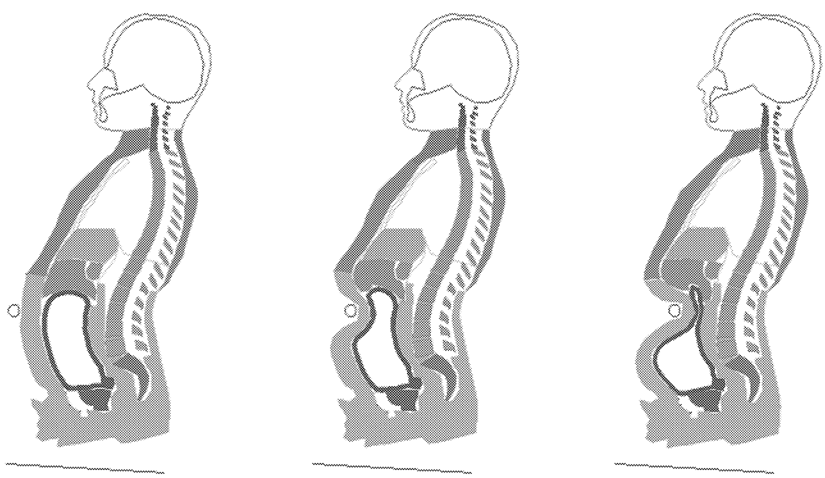

Fig.7: Low speed frontal test at time 0 ms, 10 ms and 18 ms (medial cross-section)

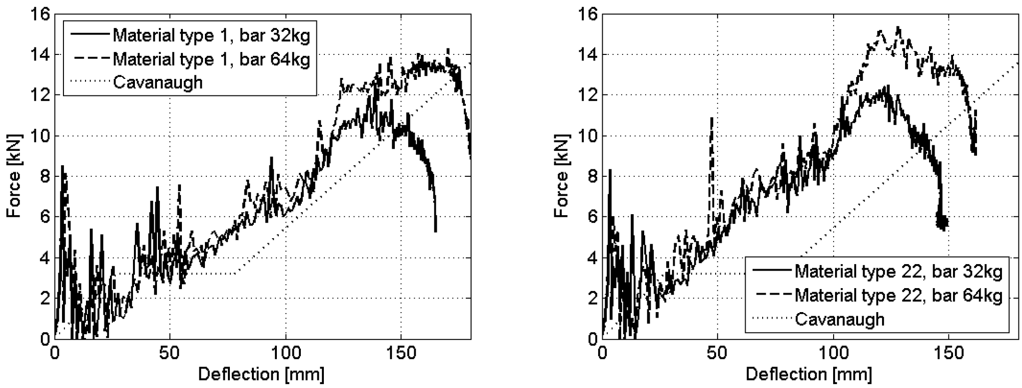

Fig.8: Results of the Cavanaugh frontal test, speed equal to 10.4 m/s, uterus modeled using material type 1 (left) and material type 22 (right)

The deflection-force dependence for the frontal test with speed equal to 10.4 m/s and uterus modeled using material type 22 shows linear dependence between the rigid bar penetration and abdominal force response for both masses of the rigid bar (see Fig. 8 right). Both dependencies are almost the same until the deflection reaches approximately 100 mm, when the higher rigid bar mass causes the slight increase of the force and the longer evolution of the dependence.

The force during the frontal test performed with speed equal to 10.4 m/s is significantly increased when the uterus is modeled using material type 22 compared to the one with uterus modeled using material type 1 (see Fig. 8). Again, the usage of material type 1 leads to the curve with more significant plateau corresponding to the Cavanaugh corridor.

Both materials show similar results, the visco-elastic material shows higher values concerning curve peak, i.e. it shows higher injury probability. Since the visco-elastic model describes the material in more realistic way, and taking into account the higher injury probability, this material should be used for further analysis.

4.3. INRETS lateral test on abdomen

The whole deformable abdominal model is validated on INRETS (Institute National de Recherche sur les Transport et leur Sécurité in France) experimental tests [2].

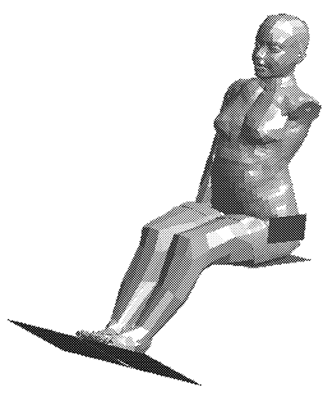

Fig.9: The INRETS lateral test setup (left arm is not displayed)

A rigid plate of size 10×20 cm and mass 23.4 kg attacks the body in the pelvis area. A contact force between the plate and the human body is measured and compared to experimental corridors provided by INRETS. Fig. 9 shows the test setup.

The test is performed for the low speed impact 3.46 m/s and the high speed impact 6.66 m/s. The resulting time-force dependencies are filtered by batch filter with low cutoff frequency equal to 0 and the vectors are for the filtration extended by 100 points. The high cutoff frequency is chosen from the interval $\langle 0.15, 0.3\rangle$ so that the resulting filtered curve corresponds the best to the original unfiltered data.

In the case of speed equal to 3.46 m/s, the force peak and the force evolution corresponds to qualitatively the INRETS corridor, but the force is delayed in time (see Fig. 10 left). It is probably caused by the pelvic flesh geometry. The layer of the flesh covering the space between the femur and the impactor is more thick because the pregnant female body holds more water and therefore it is more thick. In the case of speed equal to 6.66 m/s, the force peak and the force evolution corresponds to the INRETS corridor qualitatively. The force delay is not that significant, because the flesh is passed more quickly (see Fig. 10 right). The peak over the corridor is probably caused by the fact that the lower part of the femur is modeled as rigid and hence, without any energy absorption.

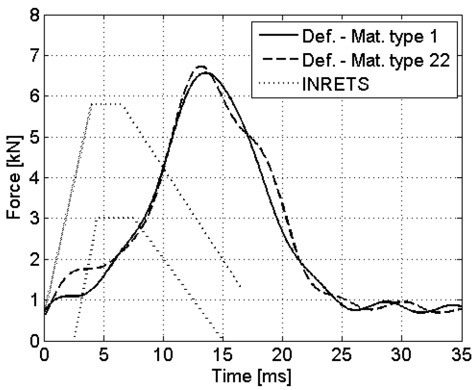

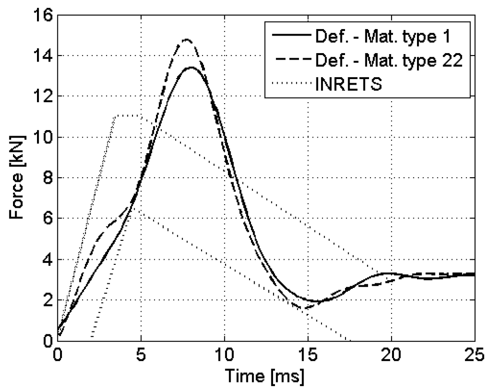

Fig.10: Force during the INRETS lateral test, speed equal to 3.46 m/s (left) and 6.66 m/s (right)

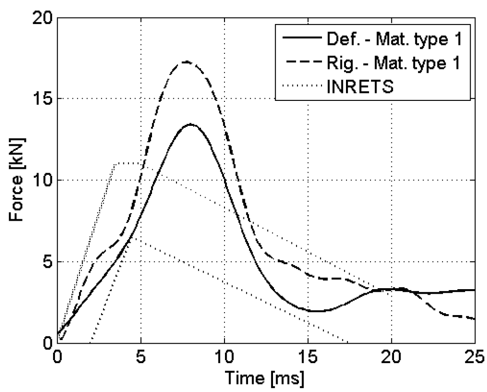

Fig.11: Comparison of the force during the high speed lateral test performed with the deformable and the rigid femur

Fig. 11 shows the difference in the force between the usage of the deformable femur model (upper part) and the rigid one. The usage of the rigid femur model causes about 30 % increase of the force in the same impact test. It seems that full deformable femur would help much more to fit the results to the corridor.

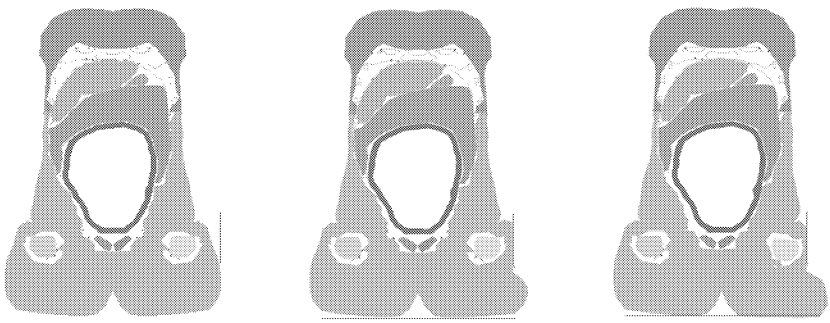

Fig.12: Low speed INRETS lateral test at time 0 ms, 7 ms and 15 ms (frontal cross-section)

5. Safety analysis

One of the pregnant female model application is the analysis of pregnant female safety during the car accident. The model is seated in the car seat and various combinations of the car interior including the steering wheel, airbag and seat belt are applied. The frontal impact of the car is simulated at the initial velocity 13.6 m/s that is equal to the car speed of 48.96 km/h. All simulations are performed with the deformable variant of upper femur and for both material types used for the uterine wall tissue modeling.

5.1. Airbag

In the first case the car interior with airbag is used. High sub-marining of the model due to the pregnancy and hence more rigid abdomen occurs. This might be caused by the stiffness of the pregnant abdomen. Unfortunately, there no real data with pregnant occupant to compare.

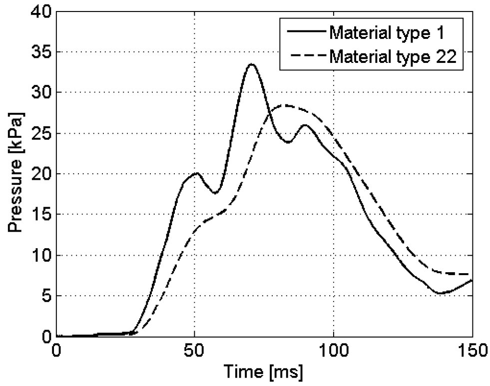

Fig.13: Pressure inside uterus during the simulation with airbag

As visible on Fig. 13, both curves have similar behaviour concerning the major peak and development. The curve is smoother in the case for visco-elastic material. The most significant difference is in the peak pressure, that is higher for the elastic-plastic material.

5.2. Various positions of the seat belt

In the second case two different positions of the seat belt are used without the car interior. The first position of the belt is the same as in the case of the previous simulation. The influence of airbag on the pressure in the uterus can be deduced from this simulation. The airbag impacts the abdomen during the simulation and therefore the pressure is higher if the airbag is used (see Figs. 13 and 14).

Similar test was performed on baboons by Snyder et al. [17]. This work presented the uterine pressure as the injury criterion. The curve describing the pressure evolution during the sled test (see Fig. 15) is comparable to the curve resulting from this simulation (see Fig. 14). The speed of the sled test with baboon was 62.1 ft/sec that corresponds to 18.93 m/s. One reason of the higher pressure peak in the sled test is that this speed is higher than used during the simulation. The second reason is that there is used only the lap belt that is placed higher over the abdomen than in our case.

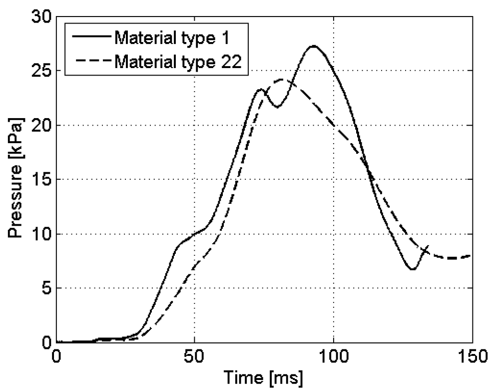

Fig.14: Pressure inside uterus during the simulation with re-positioned belt – variant 1

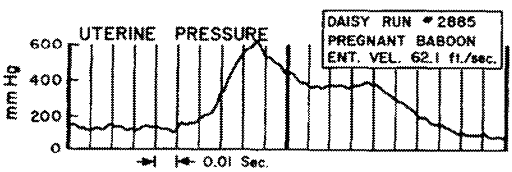

Fig.15: Pressure inside the artificial uterus during the sled test with baboon (1 mm Hg = 133.3 Pa, taken from [17])

The second seat belt used for the simulation has the upper shoulder belt fixing point moved higher and the other fixing points lower than the first seat belt. The lap belt is placed below the abdomen. As visible on Fig. 16, both curves correspond to each other. Again, the curve is smoother in the case of visco-elastic material. In this simulation, the peak pressure is higher in the case of use the visco-elastic material, but the difference is not significant. The peak pressure is smaller than in the previous simulation. It is caused by the fact that the lap belt is placed as low as possible bellow the abdomen whereas in the first case the lap belt is placed slightly over the abdomen. The pressure decrease inside the uterus can be visible comparing Fig. 14 and Fig. 16.

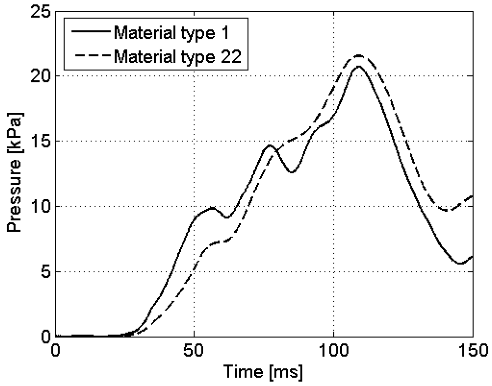

Fig.16: Pressure inside uterus during the simulation with re-positioned belt – variant 2

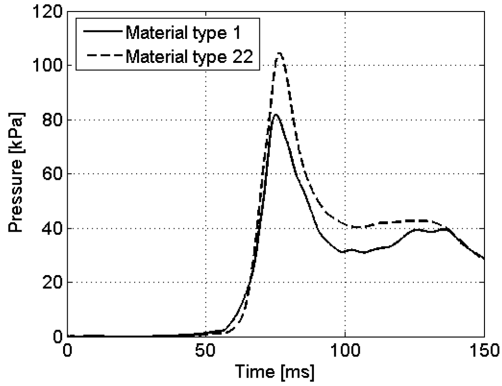

Fig.17: Pressure inside uterus during the simulation without safety restraints

5.3. No safety restraint

Last simulation performed with the pregnant female model is the simulation with the car interior without the use of the seat belt and airbag. The pressure inside the uterus is about 3 to 4 times higher than with the use of the seat belt (see Fig. 17). It is caused by the straight impact of the steering wheel that occurs at time equal to 60 ms. This impact is followed by the direct contact of the knees with the desk at time 75 ms. The head breaks the window at time 100 ms and finally the body falls at the steering wheel. These moments are shown at Fig. 18.

6. Conclusion

The creation of biomechanical human model in the PAM environmentis described. The finite element mesh symbolizing particular abdominal organs and tissues is based on the CT data obtained from the Visible Human Project [23] and the CT data of 30 weeks pregnant female obtained from [22]. The triangular surface mesh is generated with the aid of a specialized software *Amira*. Created meshes are loaded into *HyperMesh*® software where they are fitted into *ROBINA* model. Then the hexahedral mesh of each abdominal organ and tissue is created manually. The contents of the uterus are substituted by an amniotic fluid and modeled by a biobag. The uterine wall is formed by one layer of solid mesh. Two variants of femur model are created – the rigid one and the deformable one.

The pregnant female abdomen model is validated on experimental tests – Cavanaugh frontal test and INRETS lateral test. The abdominal response with the uterine wall tissue material model based on identification is compared to the one with material properties found in available sources. The results of Cavanaugh frontal test show that the material based on identification has higher dynamical rigidity.

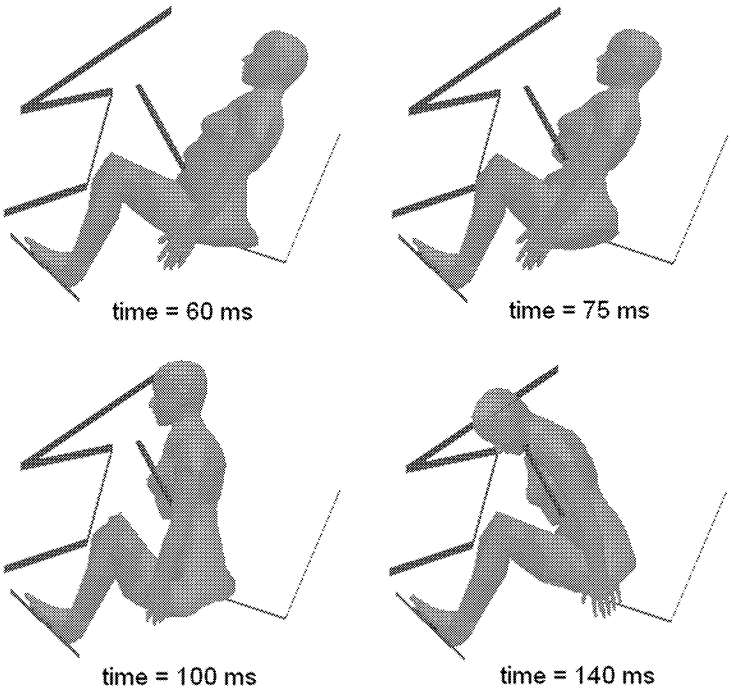

Fig.18: The simulation with no safety restraint

Two material used for the modeling of uterus are tested, namely the elastic-plastic material and the visco-elastic material. Both materials show similar results, the visco-elastic material shows higher values concerning curve peak, i.e. it shows higher injury probability. Since the visco-elastic model describes the material in more realistic way, and taking into account the higher injury probability, this material should be used for further analysis.

The practical use of pregnant female model is demonstrated on several types of sled tests. As expected, the most safe variant for the mother seems to be the use of the seat belt and airbag. From the simulations stated above, the most safe variant of the fetus seems to be the seat belt only, because the airbag impacts the abdomen during simulation that increases the pressure inside the uterus. The significant role is played by the placement of the lap belt. It should be placed bellow the abdomen, across the hips and over the pelvis. The injuries suffered when using no safety restraint seem to be fatal for both mother and fetus.

Acknowledgment

The work is supported by the Ministry of Industry and Trade, project FT-TA/024. Special thanks belong to ESI Group International and John H. and Any Bowles Foundation.

References

[1] Beaugonin M., Haug E., Hynčík L.: ROBBY2 – α-version, ESI SA 1998

[2] Bouquet R., Ramet M., Bermond F., Cesari D.: Thoracic and Pelvis Human Response to Impact, Proc. 14th International Technical Conference on the Enhanced Safety of Vehicles, Vol. 1, 1994, pp. 100–109

[3] Cavanaugh J.M., Nyquist G.W., Goldberg S.J., King A.I.: Lower Abdominal Impact Tolerance and Response, Proc. 30th Stapp Conference, SAE Technical Paper No. 861878, 1986

[4] Cunningham F.G., Gant N.F., Leveno K.J., Gilstrap L.C., Hauth J.C., Wenstrom K.D.: Williams Obstetrics, 21st ed., New York, McGraw-Hill, 2001, ISBN 0-07-112195-1 (international), 0-8385-9647-9 (domestic)

[5] Degani S., Leibovitz Z., Shapiro I., Gonen R., Ohel G.: Myometrial thickness in pregnancy: Longitudinal sonographic study, Journal of Ultrasound in Medicine, Vol. 17, Issue 10, 1998, pp. 661–665, ISSN 0278-4297

[6] Duma S., Moorcroft D., Stitzel J., Duma G.: A Computational Model of the Pregnant Occupant: Effects of Resrtaint Usage and Occupant Position on Fetal Injury Risk, United States, Paper Number 05-0367,
Available on: www-nrd.nhtsa.dot.gov/pdf/nrd-01/esv/esv19/05-0367-O.pdf

[7] Eppinger R.H.: Prediction of thoracic injury using measurable experimental parameters, Proceedings of the Sixth International Technical Conference on Experimental Safety Vehicles, United States Department of Transportation, NHTSA, Washington D.C., 1976, pp. 770–780

[8] Eppinger R.H., Marcus J.H., Morgan R.M.: Development of dummy and injury index for NHTSA's thoracic side impact protection research program. SAE Technical Paper No. 840885

[9] Hynčík L.: Biomechanical Model of Abdominal Organs and Tissues for Car Crash Test Purposes, Ph.D. Thesis, University of West Bohemia in Pilsen, Pilsen, 2002

[10] Hynčík L., Beneš K., Jirkovský J., Smejkal J., Voborská V.: Biomechanical Human Model, Conference B of 8th European Automotive Congress, Bratislava, 2001

[11] Jansová M.: Biomechanical Model of Pregnant Female for Impact Purposes, disertační práce, ZČU v Plzni, 2007

[12] Jansová M.: Biomechanical Model of the Knee Joint Menisci, Diploma Thesis, University of West Bohemia in Pilsen, Pilsen, 2003

[13] Lopot F., Kubový P., Jelen K., Nováček V., Budka Š., Doležal A.: Experimental Identification of Basic Material Properties of Muscle of Uretrine Wall, EMBEC'05, Prague, 2005

[14] Moorcroft D., Stitzel J., Duma G., Duma S.: Computational Modeling of a Pregnant Occupant, http://www.automotive.tno.nl/Madymo/Publications/UMAmericas2003/

[15] PAM-CRASH/SAFE® Reference And Solver Notes Manuals, Version 2005

[15] Rupp J.D. et al.: Development and testing of a prototype pregnant abdomen for the small-female Hybrid III ATD, Stapp Car Crash Journal, Vol. 45, 2001, pp. 61–78, ISBN 0-7680-0918-9

[16] Snyder R.G., Snow C.C., Crosby W.M., Hanson P., Fineg J., Chandler R.: Impact Injury to the Pregnant Female and Fetus in Lab Belt Restraint, 10th Stapp Conference, SAE Technical Paper No. 660801, 1966

[17] Williams P.L. et al.: Gray's Anatomy, 38th ed., Churchill Livingstone, 1995, ISBN 0-443-05717-6

[18] Altair® HyperMesh®7.0, www.altair.com/software/hw_hm.htm

[19] Amira, www.amiravis.com

[20] ESI Group, www.esi-group.com

[21] Rensselaer Radiation Measurement & Dosimetry Group, Troy, New York, www.rpi.edu/dept/radsafe/public_html/index.htm

[22] The Visible Human Project®, http://www.nlm.nih.gov/research/visible

Received in editor's office: November 30, 2007
Approved for publishing: July 24, 2008

Note: The paper is an shortened version of Ph.D. thesis [11].